Bull. Chem. Soc. Ethiop. **2025**, 39(4), 643-657.
DOI: https://dx.doi.org/10.4314/bcse.v39i4.4

ISSN 1011-3924
Printed in Ethiopia
Online ISSN 1726-801X

INVESTIGATING THE COMPARATIVE ADSORPTION OF METHYL ORANGE AND METHYL GREEN ON COMMERCIAL BENTONITE

Houria Rezala[1*], Amaya Romero[2] and Naoual Tidjani[3]

[1]Laboratoire de Valorisation des Substances Naturelles, Faculté des Sciences et de la Technologie, Université Djilali Bounaama de Khemis-Miliana, Route de Theniet El Had, 44225 Khemis-Miliana, Algérie
[2]Department of Chemical Engineering, Higher Technical School of Agronomical Engineers, University of Castilla-La Mancha, Ronda de Calatrava 7, E-13071, Ciudad Real, Spain
[3]Electronic Department, Blida University, Road of SOUMÂA PO Box 270, 09000 Blida, Algeria

(Received June 5, 2024; Revised December 31, 2024; Accepted January 3, 2025)

ABSTRACT. This paper presents the utilization of commercial bentonite obtained from Biochem Chemopharma Company, in France, as an adsorbent for the anionic dye methyl orange (MO) and cationic dye methyl green (MG) in aqueous solutions. The material was analyzed using X-ray fluorescence (XRF), Fourier transform infrared spectroscopy (FTIR), and X-ray diffraction (XRD). Nitrogen adsorption at 77 K and thermogravimetric analysis (TGA) were performed for characterization. The study evaluated the impact of various experimental parameters such as contact time, solution pH, adsorbent dose, initial dye concentration, and temperature. Batch adsorption studies revealed that MO exhibited a maximum of 90 mg/g in an acidic medium, with an equilibrium time of 20 min and an adsorbent dosage of 1 g/L. On the other hand, MG demonstrated maximum adsorption of 165 mg/g in a natural medium, with an equilibrium time of 5 minutes and an adsorbent dose of 0.6 g/L. The adsorption of MO followed a pseudo-first-order kinetic model and the isotherms were well-fitted by the Freundlich model for MO and both Freundlich and Langmuir models for MG. Thermodynamic analysis indicated an exothermic, spontaneous, and physical adsorption process. Lastly, the adsorption performance of commercial bentonite for MO was compared with that of MG.

KEY WORDS: Methyl orange, Methyl green, Commercial bentonite, Adsorption, Isotherm models, Kinetic models

INTRODUCTION

The dyes of particular relevance are utilized in numerous industries, including the textile, paper, leather, food, and cosmetics industries [1]. These companies may release colored wastewater, which could be hazardous to the environment and threaten bioaccumulation. These dyes are also more soluble in water and exhibit good stability against oxidants, heat, and light [2]. Dye pollutant concentrations can be exceedingly detrimental to aquatic environments, even at low levels [3]. Depending on the ion load of their molecules, dyes are categorized as cationic, anionic, or nonionic. In comparison to anionic dyes, cationic dyes are more hazardous.

Methyl green (MG) is a dicationic dye that belongs to the triphenylmethane family and is utilized in different applications, including textile dying, medicine, and staining paper [2]. It is toxic to aquatic organisms, severe skin burns and eye damage, causes long-term adverse effects, and irritates the respiratory tract. Research labs, the textile industry, and the printing paper-making process frequently utilize methyl orange (MO), an anionic dye. It can have adverse consequences on people, including vomiting, cyanosis, diarrhea, elevated heart rate, and tissue necrosis [4]. Thus, before their release into the environment, adequate previous treatment is unquestionably required [5].

*Corresponding authors. E-mail: rezala_houria@hotmail.com

Several techniques have been used to remove dyes from contaminated wastewater, such as photocatalysis, chemical oxidation, ion exchange, membrane, filtration, peroxi-coagulation and peroxi-electrocoagulation, biodegradation and adsorption [2, 4, 6]. Adsorption is widely utilized and simple due to its accessibility, affordability, and high efficacy [7]. Currently, many adsorbents have been used to remove these dyes from water, including activated carbon [8], zeolite [3, 9], graphene [10], metal-organic frameworks [11], clays, and modified clays [12].

Numerous studies have extensively explored the use of clays for the adsorption of organic dyes due to their cost-effectiveness, abundance in nature, and high efficiency. Among these clays, bentonite has gained significant recognition as an effective adsorbent. Currently, various commercial bentonite products are available in the market. Commercial bentonite has demonstrated improved removal efficiency for substances such as carbendazim [13], aflatoxins [14], pyrene [15], and manganese [16]. However, only one existing report on using commercial bentonite was obtained from Biochem Chemopharma Company for adsorption purposes [17]. This study compared the adsorption of MB using nickel oxide-modified montmorillonite and commercial bentonite, with the results indicating that commercially available bentonite outperformed the nickel oxide-modified montmorillonite.

This study aimed to utilize commercial bentonite obtained from Biochem Chemopharma Company for the adsorption of MG and MO. The adsorbent was characterized using XRF, FTIR, XRD, nitrogen adsorption at 77 K, and TGA. Batch adsorption experiments were conducted to investigate the effects of contact time, adsorbent mass, solution pH, initial dye concentration, and temperature. The kinetics and isotherms of the adsorption process were determined. Additionally, the adsorption performance of commercial bentonite for the anionic dye MO was compared to that of the cationic dye MG.

EXPERIMENTAL

Materials and chemicals

The Biochem Chemopharma company (France) provided the dyes MG (chemical formula $C_{27}H_{35}Cl_2N_3$. $ZnCl_2$, molecular weight = 608.79 g/mol, λ_{max} = 630-635 nm, solubility in water = 1 g/L), and MO (chemical formula $C_{14}H_{14}N_3NaO_3S$, molecular weight = 327.34 g/mol, λ_{max} = 466 nm, solubility in water = 5 g/L), as well as chemicals (NaOH, H_2SO_4) and commercial bentonite. These were utilized exactly as received, requiring no additional purification. Distilled water was used to prepare all of the solutions.

Characterization methods

The chemical composition of the commercial bentonite was determined by X-ray fluorescence spectrometry (PHILIPS-PW2404 Pananalytical, Magix-Pro model) of 4 kW of power. Semi-quantitative measurements were made with the Ommian application using 27 mm sample holders with a full range measurement sweep. The Fourier transform infrared (FTIR) of the samples was obtained using a SPECTRUM TWO spectrometer (Perkin Elmer, Inc.), while ZnSe (550–6000 cm^{-1}) and KBr (350–8300 cm^{-1}) pellets were used. The XRD study was obtained using a diffractometer (PHILIPS, PW-1711) equipped with CuKα radiation (l = 0.15404 nm). Using nitrogen as the sorbate gas at 77 K, the textural qualities were measured using a Quantachrome Quadrasorb SI system. The samples were outgassed for 18 h at 373 K under a high vacuum (10^{-2} Torr). Total surface areas were calculated using the multipoint BET method and pore size distributions with BJH using N_2 adsorption/desorption data [18]. The thermal stability of the generated aerogels was assessed using a thermal analyzer (TGA, 2STARe System, Mettler Toledo) at a heating rate of 10 °C min^{-1} in an air environment.

Adsorption experiments

For the adsorption experiment, a water bath shaker was used to perform tests with a constant speed of 150 rpm by mixing in glass vials a series of 25 mg of commercial bentonite with a series of 25 mL of initial dye solutions at 100 mg/L. The material's adsorption properties were examined during a time ranging from 5 to 90 min, solution pH (2 - 10), adsorbent dose (0.2 – 4 g/L), initial concentrations of dyes (4 - 100 mg/L) and temperature (20 – 50 °C) for optimizing operating conditions. The experiment was conducted three times to assess the error, which consistently fell within the ± 5% range around the mean values. As the adsorption experiment concludes, the adsorbent was separated from the solution by centrifuging the commercial bentonite-dye system to centrifugation at 1500 rpm for 20 min. The liquid portion is a UV-Vis spectrophotometer (UV-3100, J. P. Selecta, Spain) at the highest wavelength of 466 nm and 632 nm for MO and MG, respectively. Calibration curves were utilized to determine the dye concentration in each experiment, wherein the absorbance was plotted against the dye concentration.

The pH levels of dye solutions were modified by introducing a few drops of H_2SO_4 aqueous solutions (0.1 mol/L) and NaOH (0.1 mol/L) and subsequently assessed using a pH meter (Basic 20+, Crison Instruments S. A., Spain). The experimental procedure involved the addition of 25 mg of commercial bentonite to 25 mL of dye solutions with varying concentrations ranging from 4 to 200 mg/L for desired contact time and pH. The equilibrium amounts of adsorbed dye per unit mass of the sample, denoted as q_e (mg/g), and the removal efficiency of the dye, denoted as E (%), were determined using equations (1) and (2), respectively.

$$q_e = V\,(C_0 - C_e)/m \quad (1)$$

$$E(\%) = 100\,(C_0 - C_e)/C_0 \quad (2)$$

where C_0 represents the starting concentration of dye (mg/L), C_e is the equilibrium concentration of dye (mg/L), V is the volume of dye solution (L), and m is the mass of commercial bentonite (g).

RESULTS AND DISCUSSION

Commercial bentonite characterization

The X-ray fluorescence results for commercial bentonite are shown in Table 1. The main oxides are SiO_2 (47.7%) and Al_2O_3 (17.9%), indicating that this adsorbent belongs to aluminosilicate materials. Fe_2O_3 (7.8%) also plays a role in the sample's coloration. Other oxides are present in small percentages. The bentonite is predominantly sodium montmorillonite (sodium type) due to its Na^+ content, which aligns with previous findings [14, 19] on commercial bentonite from South Oil Company and Argentinean bentonites.

Table 1. X-ray fluorescence for commercial bentonite.

Compound	Na_2O	MgO	Al_2O_3	SiO_2	P_2O_5	SO_3	Cl	K_2O	CaO
Weight (%)	2.429	2.986	17.863	47.701	0.084	0.699	0.387	0.875	1.014
Compound	TiO_2	V_2O_5	Cr_2O_3	MnO	Fe_2O_3	Co_3O_4	NiO	CuO	ZnO
Weight (%)	1.798	0.024	0.026	0.052	7.821	0.015	0.013	0.010	0.011
Compound	Ga_2O_3	Br	Rb_2O	SrO	Y_2O_3	ZrO_2	Nb_2O_5	BaO	Loss on ignition
Weight (%)	0.004	0.001	0.004	0.027	0.004	0.037	0.004	0.011	16.103

The characteristic functional groups of the commercial bentonite were investigated using the FTIR technique. The spectra in the range of 4000–400 cm^{-1} are shown in Figure 1a. The vibrations of the Si-OH bond result in a band at 3690 cm^{-1}. The band at about 3625 cm^{-1} corresponds to the stretching vibration of octahedral O-H groups, attached to Al^{3+} or Mg^{2+} [20]. The band at 1632 cm^{-1} corresponds to the H–O–H deformation vibrations of water. The most intense band at 997 cm^{-1} is attributed to the asymmetric Si–O–Si stretching vibrations of the tetrahedral sheet. The occupancy of the octahedral sheets is indicated by the 913 cm^{-1} band, representing Al–Al–OH bending vibrations. The montmorillonite is characterized by the bands at 516 and 461 cm^{-1}, corresponding to the bending and stretching vibrations of Si-O bonds.

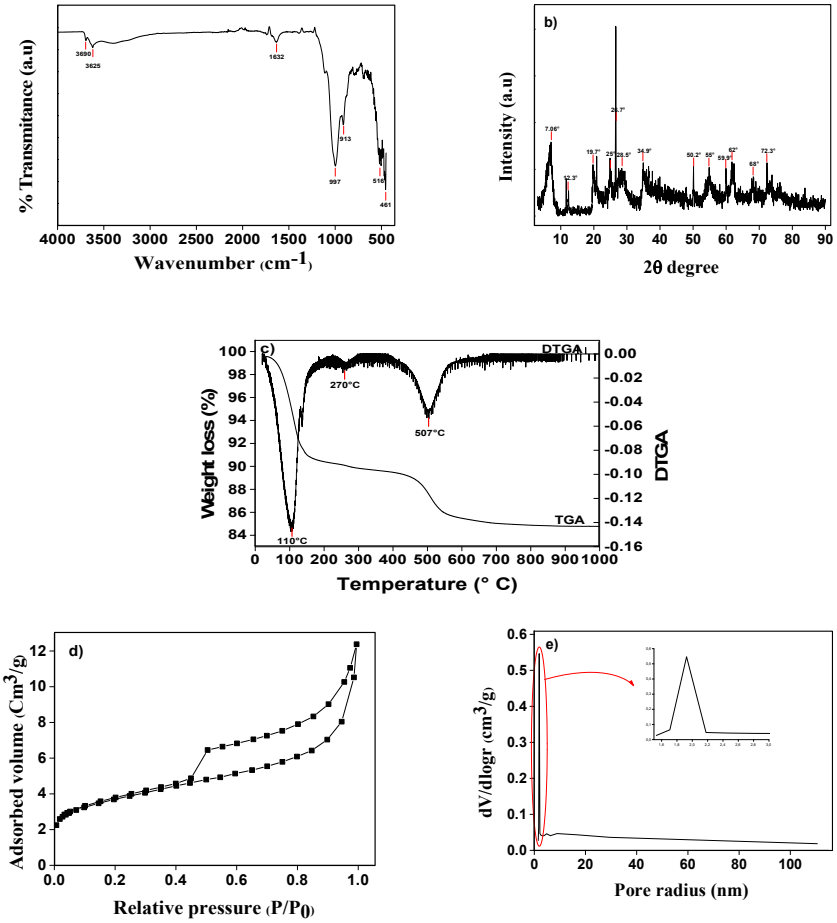

Figure 1. The commercial bentonite's a) FTIR spectra. b) XRD patterns. c) TGA and DTG curves. d) N_2 adsorption-desorption isotherms. e) Pore size distribution.

The XRD patterns and relative basal spacing of the commercial bentonite are shown in Figure 1b and Table 2. The major peaks correspond to montmorillonite, with diffraction angles 2θ at around 7.1º, 12.3º, 19.7º, 28.5º, 34.9º, 55º, 62°, and 72.3°. The d_{001} value of the basal bentonite

peak (12.55 Å) suggests that the main interlayer cation is sodium, consistent with the XRF analysis. Similar findings have been previously reported in the literature [4, 7, 19, 21]. Other peaks observed are impurities such as kaolinite with diffraction angles 2θ at 25º, and quartz or SiO_2 with diffraction angles 2θ at 26.7º, 50.2º, 59.9º, and 68º.

Thermal gravimetric and derivative thermal gravimetric curves of commercial bentonite are presented in Figure 1c. The TG curves exhibit continuous mass loss and could be divided into three sections. The first substantial reduction in mass has been seen within the temperature range of 25-200 °C, with the DTG peak centered at 110 °C. This peak is characteristic of sodium montmorillonite and is attributed to the loss of adsorbed water, and can be prolonged up to 250 ºC [22]. The second small mass loss in the temperature range of 200-300 °C with a DTG peak centered at 270 °C could be attributed to the loss of interstitial water bound by hydrogen bonds [23]. The temperature ranges of 400-600 °C exhibit a third mass loss, with the DTG peak centered at 507 °C, which is correlated with the sodium ions within the interlayer cavity [23].

The nitrogen adsorption-desorption isotherm of commercial bentonite is shown in Figure 1d. When the relative pressures were low ($p/p_0 < 0.05$), the isotherm exhibited type I isotherms as classified by Brunauer, Deming, Deming, and Teller (BDDT) [24], which is characteristic of microporous systems [25]. Nevertheless, the isotherm is correlated with the type IV class when the p/p_0 value is greater, indicating that the system has a wide range of pore sizes. The identification of hysteresis loops, type H3 as described by Sing *et al.* [25], suggests the existence of mesoporosity inside this material. The mesopore distribution for the sample was determined using the Barret-Joyner-Halenda (BJH) method). Figure 1e shows commercial bentonite is characterized by an unimodal pore size distribution with a maximum radius of 1.92 nm. The textural properties of the commercial bentonite are shown in Table 2. The specific surface area of the commercial bentonite used is 77 m^2/g. This value is higher than that reported by [12, 26]. Thus, the micropore surface area, micropore volume, and pore volume are higher than Algerian bentonite [7].

Table 2. Basal spacing (d_{001}) and textural properties of commercial bentonite.

Basal spacing d_{001} (Å)	BET surface area (m^2/g)	Micropore surface area (m^2/g)	External surface area (m^2/g)	Micropore volume (cm^3/g)	Pore volume (cm^3/g)
12.55	76.97	27	49.97	0.013	1.15

Dyes adsorption

The influence of contact time on the adsorption of dyes is a crucial determinant of the equilibrium time. The adsorbed amounts of both dyes as a function of contact time are depicted in Figure 2a. Two stages of dye uptake were observed. During the early stage, the removal of MG and MO occurred rapidly, within ($t < 5$ min and $t < 20$ min for MG and MO, respectively). This can be attributed to the abundance of active sites that were available for adsorption. In the second stage (from 5 to 90 min and from 20 to 90 min for MG and MO, respectively), the adsorption amount remained constant as the active sites became saturated. The final adsorption capacities were calculated to be approximately 79 mg/g for MO and 99 mg/g for MG. No further adsorption was observed beyond this point. Therefore, a contact time of 5 min for MG dye and 20 min for MO dye was deemed sufficient for subsequent experiments. This equilibrium period surpasses previously reported values [4, 27].

The kinetic of MG adsorption by commercial bentonite was not carried out because the adsorbed amount was very fast and reached equilibrium within the first 5 min. The kinetics process has been modeled using pseudo-first-order and pseudo-second-order models to examine the kinetics and mechanism of MO adsorption on commercial bentonite. The linear form of the pseudo-first-order equation [28] is given by:

$$\log(q_e - q_t) = \log q_e - k_1 t / 2.303 \quad (3)$$

The expression of the linear form of the pseudo-second-order model [29, 30] is given as:

$$t/q_t = 1/k_2 q_e^2 + t/q_e \quad (4)$$

The MO (mg/g) adsorbed on the adsorbent at equilibrium and at a specific time t (min) are denoted as q_e and q_t, respectively. The k_1 (min^{-1}) and k_2 (g/mg.min) represent the Pseudo-first-order and pseudo-second-order rate constants, respectively. The kinetic fit curves are shown in Figures 2b and 2c. Table 3 presents the kinetic parameters and correlation coefficient data. The pseudo-first-order model demonstrated a strong match with the experimental results, as indicated by an R^2 value of 0.998. In addition, the obtained q_e value of 82 mg/g from the pseudo-first-order model closely approximated the experimental value of 79 mg/g, hence demonstrating the model's efficacy in accurately representing the MO data.

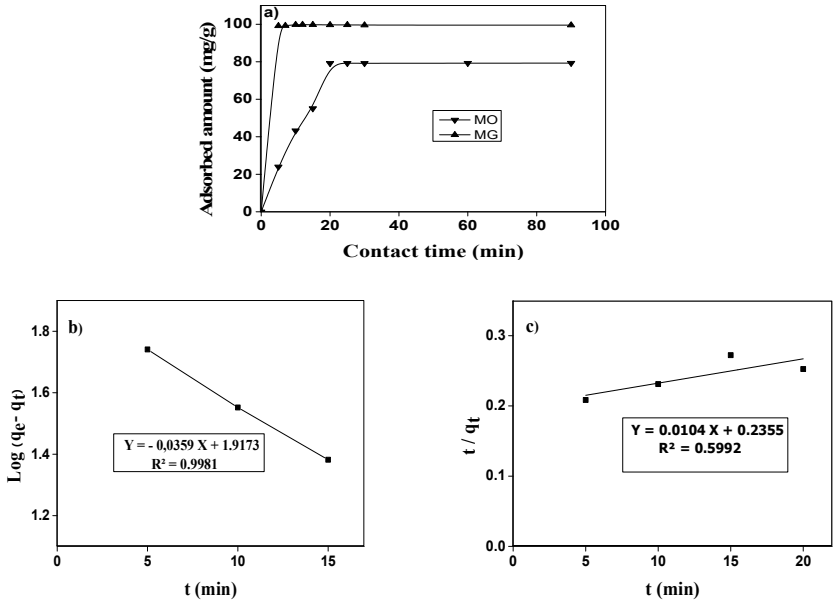

Figure 2. a) Effect of contact time on MO and MG removal onto commercial bentonite (adsorbate concentration: 100 mg/L, adsorbent dose: 1 g/L). b) pseudo-first-order model for the adsorption of MO by commercial bentonite. c) pseudo-second-order model for the adsorption of MO by commercial bentonite.

Table 3. Adsorption kinetic parameters of MO on commercial bentonite.

Adsorbent	Pseudo-first-order model			Pseudo-second-order model		
	q_e (mg/g)	k_1 (min^{-1})	R^2	q_e (mg/g)	k_2 (g/mg.min)	R^2
Commercial bentonite	82.66	0.082	0.998	96.15	$4.59 * 10^{-4}$	0.60

The pH of the solution is an essential parameter in all sorption studies because it affects the surface charge of the adsorbent and the degree of ionization and speciation of the adsorbate. The impact of the pH of the solution on commercial bentonite has been studied, and the results are shown in Figure 3a. The point of zero charge (pH_{pzc}) is an important parameter that indicates surface charge [7]. In this study, the effect of pH was studied in the ranging from pH 2 to 10. The adsorbent surface exhibits a negative charge when the pH of the solution is greater than the pH_{PZC} and a positive charge when the pH of the solution is less than the pH of the pHpzc [31]. The pH_{pzc} of the commercial bentonite was found to be 2.4. For pH > 2.4, the surface of the commercial bentonite becomes negatively charged and the dye's structure varies depending on the medium in which it is present, whether it is an acid or basic solution. For pH < pK_a = 3.4, the MO dye exists mainly in its protonated form (it was present as a sulfonic acid or quinone structure) while for pH > pK_a, it loses its protons and changes to its deprotonated form (pH > 4.4), it was present as a sodium sulfonate salt (azo structure), as shown below:

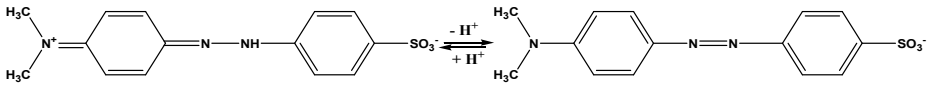

MO (Quinone structure) **MO (Azo structure)**

The adsorption capacity of MO is maximum at pH 2 (< 3.4). At the pH range of 2-3.4, there was strong adsorption, due to the electrostatic interactions between the N-positive ion which can become a new adsorption site of the quinone structure of MO with the negatively charged of the commercial bentonite. At the pH range of 3.4-4.4, there was a slight adsorption attributed to the existence of the two MO forms (quinone and azo structures). On the contrary, the increasing pH solution, from 4.4 to 10 caused a decrease in the adsorption capacity of adsorbent, resulting in electrostatic repulsions between the negatively charged surface of commercial bentonite and the negative charges of MO (azo structure). Similar results have been reported by previous works [4, 32, 33].

Furthermore, it is known that methyl green has a divalent cation MG^{2+} in an acidic solution and has a monovalent cation ($carbinol^+$) in in neutral or basic solution [34], as shown below:

$$MG^{2+} + OH^- \leftrightarrow carbinol^+$$

It is seen that there was a high adsorption capacity of MG for the entire pH (from 2 to 10) region and this can be due to the high electrostatic attractions between the positive charges of MG molecules and the negatively charged surface of the adsorbent. Similar results were obtained for the adsorption of methygreen by polymeric resins [35]. According to these results, the optimum pH of 2 is fixed for MO and retained the pH solution without adjustment for MG in the rest of the adsorption experiments.

Another important parameter in dye adsorption is the adsorbent dose. The impact of the adsorbent dose on the adsorption capacity of MO and MG is depicted in Figure 3b. Initially, the adsorption process increases with an increase in adsorbent mass, attributed to a higher number of active sites. However, after reaching an optimal dose of 90% for MO and 99% for MG, the adsorption capacity remains constant. Further, the inclusion of additional adsorbent does not yield a substantial impact on the adsorption process, potentially attributable to the occurrence of adsorption site overlap resulting from the dense arrangement of adsorbent particles [36, 37]. Therefore, an optimum dose of 0.6 g/L for MG and 1 g/L for MO was selected and used in subsequent experiments.

Equilibrium investigation provides valuable information on the interactions between adsorbate and adsorbent. The study additionally establishes a correlation between the concentration of adsorbate in a solution and the quantity of adsorbate adsorbed on the surface of the adsorbent at the time that both liquid and solid phases are in a state of equilibrium [38]. The

isotherms are formed by plotting the adsorbed amount of dye versus the equilibrium concentration. Figure 4a depicts the effect of initial dye concentration as well as adsorption equilibrium isotherms of the MO and MG removal by the adsorbent. The quantity of dyes adsorbed exhibits a positive correlation with the initial concentration of the adsorbate, owing to the heightened driving force exerted by the concentration gradient [7]. Other articles have also reported similar findings for MG [10] and MO [32] dyes.

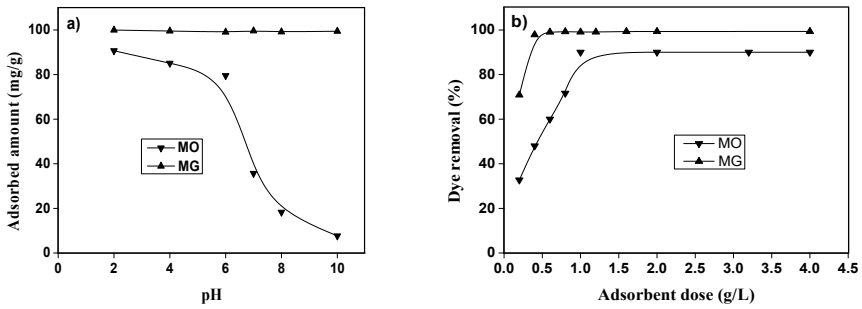

Figure 3. a) Effect of solution pH on the adsorption of MO and MG by commercial bentonite (adsorbate concentration: 100 mg/L, contact time: 20 min (MO) and 5 min (MG), adsorbent dose: 1 g/L). b) Effect of adsorbent dose on dye removal (contact time: 20 min (MO) and 5 min (MG), pH = 2 (MO), adsorbate concentration = 100 mg/L).

To better understand the adsorption mechanism by which MO and MG adhere on commercial bentonite, Langmuir [39], Freundlich [40], and Temkin [41] models were applied. The Langmuir, Freundlich, and Temkin models can be represented in their linear forms using equations (5), (6), and (7), respectively.

$$C_e/q_e = 1/k_L q_m + C_e/q_m \quad (5)$$

$$\log q_e = \log K_F + 1/n \ (\log C_e) \quad (6)$$

$$q_e = B_T \ln K_T + B_T \ln C_e \quad (7)$$

where q_m (mg/g) is the maximum adsorption capacity, K_L (L/mg) is the Langmuir constant, K_F (mg/g) and n are the Freundlich constants, K_T (L/mg) is the Temkin constant, $B_T = RT/b$, T is the temperature (K), R is the universal gas constant (8.314 J/mol K) and b is the Temkin constant related to heat of adsorption (J/mol).

Figures 4b, 4c, and 4d present the adsorption isotherm fitting plots of commercial bentonite. Table 4 displays the estimated values of the corresponding parameters.

The adsorption isotherms of commercial bentonite for MO were found to be more in line with the Freundlich model, with the highest coefficient of correlation (R^2 = 0.98) (Table 4). Additionally, for MG, the results indicate that both the Langmuir and Freundlich models fit the equilibrium data well, as evidenced by high R^2 values (0.99), suggesting that the adsorption occurs on both monolayer and heterogeneous surface conditions.

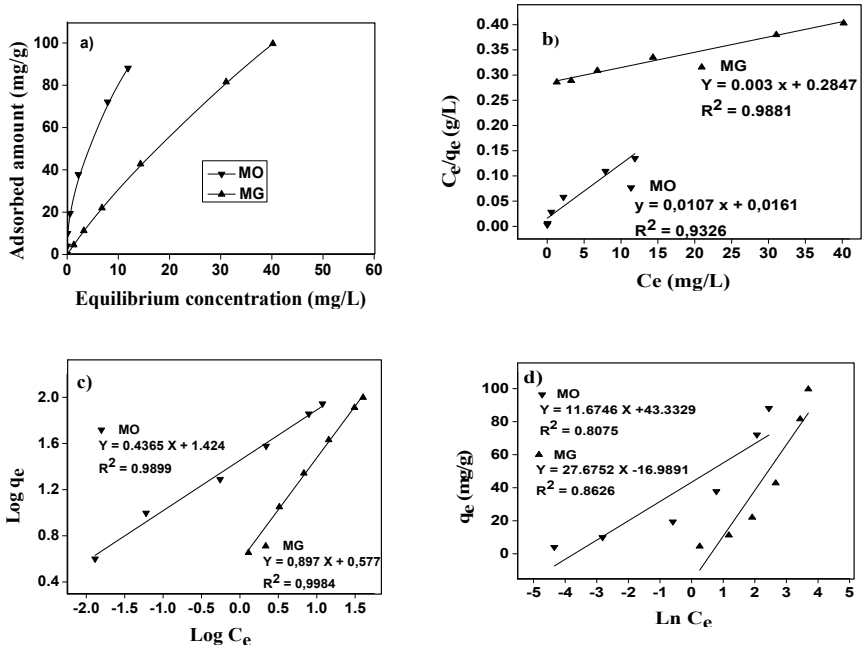

Figure 4. a) Adsorption isotherms of MO and MG onto commercial bentonite (contact time: 20 min (MO) and 5 min (MG), pH = 2 (MO), adsorbent dose: 1 g/L (MO) and 0.6 g/L (MG)). b) Langmuir model. c) Freundlich model. d) Temkin model.

The equation for calculating R_L may be determined based on K_L and the initial concentration of methyl orange C_0.

$$R_L = 1/(1 + k_L C_0) \quad (8)$$

The R_L parameter quantifies the extent of interactions occurring between adsorbate ions and the surface of the adsorbent. The adsorption process is advantageous $0 < R_L < 1$, unfavorable $R_L > 1$, linear adsorption $R_L = 1$, and irreversible adsorption $R_L = 0$ [42].

In addition, the values of the Freundlich constant (n) indicate if the adsorption process is favored or not favored: good adsorption n = 2–10, moderately difficult adsorption n = 1–2, and poor adsorption n < 1 [6]. For both dyes, n values are higher than 1 and R_L values are between 0-1, indicating the favorable adsorption of MG and MO dyes on the surface of the commercial bentonite.

The analysis of Figures 2 to 4 reveals a notably superior adsorption performance of the adsorbent towards cationic dyes (MG) in comparison to anionic dyes (MO). This behavior can be elucidated by several factors: (i) cation-exchange processes, wherein Na ions are displaced by MG adsorbed molecules; (ii) the presence of OH groups associated with the oxide layers SiO_2 and Al_2O_3, as to be rephrased by XRF analysis; (iii) interactions involving the π electronic clouds of MG and cations such as Na^+ located on the surface or interlayer of the clays (d_{001} = 12.55 Å), in alignment with findings from XRF, TGA, and XRD analyses; (iv) the formation of hydrogen bonds between the nitrogen atoms of MG and the hydrogen atoms bonded to the oxygen atoms of the silanol (Si-OH) groups in the clay, consistent with FTIR analysis; (v) electrostatic attractions

between the positively charged MG and the negatively charged surface of commercial bentonite; (vi) the presence of Van der Waals forces between MG and commercial bentonite; and (vii) electrostatic attraction between the $R\text{-}N^+$ group of the dye and deprotonated SiO^- and/or AlO^- groups on the surface of commercial bentonite.

Table 4. Isotherm model and thermodynamic parameters for the adsorption of MO and MG onto commercial bentonite.

Dye	Langmuir			Freundlich			Temkin		
	q_m (mg/g)	K_L (L/mg)	R^2	n	K_F (mg/g)	R^2	B_T	K_T (L/mg)	R^2
MO	92.93	0.66	0.93	2.32	28.44	0.989	11.67	40.85	0.807
MG	333.33	0.01	0.988	1.12	3.78	0.998	27.67	0.54	0.862

Dye	ΔH° (kJ/mol)	ΔS° (J/mol.K)	ΔG° (kJ/mol)			
			293 K	303 K	313 K	323 K
MO	-6.07	-2.82	-5.24	-5.22	-5.19	-5.16
MG	-17.90	-35.82	-7.40	-7.04	- 6.69	- 6.33

Table 5 presents a summary of the results collected from the literature on the adsorption of methyl green by different adsorbents, for comparison. The table illustrates that the commercial bentonite obtained from Biochem Chemopharma company in France has a notable affinity for MG molecules, resulting in significantly greater removal effectiveness (99%) compared to prior findings [35, 43-48]. Moreover, commercial bentonite exhibits favorable adsorption properties for the removal of MG dye due to its higher surface area, reaching 77 m^2/g, in comparison to Algerian bentonite, which is consistent with the nitrogen adsorption at 77 K. Also, the results indicated that this material causes an accelerated mass transfer rate in less contact time (5 min), this is an important economic reason from the perspective of scaling up productions for industrial applications. Furthermore, using low masses of commercial bentonite with the shortest adsorption time is economically more favorable. No pre-treatment was applied to the adsorbent in this work to increase its use.

Table 5. Comparison of MG adsorption by various adsorbents.

Adsorbent	Concentration (mg/L)	Adsorbent mass (g/L)	Time (min)	Efficiency (%)	Reference
$NiFe_2O_4$-CNTs	100	1.4	120	56.19	[43]
Loofah fibers	5	0.4	250	75.8	[44]
Bamboo	5	1	140	79.4	[45]
Bio-based chitosan/Fe_2O_3/$NiFe_2O_4$	40	2.667	60	96.51	[46]
CPAuNPs	50	0.05	180	86.02	[47]
Pomegranate Peels	100	1	70	90	[48]
Amberlite XAD-2 resin	25	0.014	150	95	[35]
Commercial bentonite (France)	100	0.6	5	99	This study

The adsorption process is significantly influenced by temperature. Figure 5a displays a graph illustrating the relationship between temperature (293, 303, 313, and 323 K) and the uptake of MO and MG. As the temperature climbed from 293 K to 323 K, the adsorbed quantities of both dyes, MO and MG, fell somewhat from 89.69 to 86.37 mg/g and 101.83 to 98.67 mg/g g, respectively. The obtained outcome suggests that the adsorption onto the commercial bentonite is advantageous under low-temperature conditions, so implying that the adsorption process is exothermic. According to Rezala *et al.*, the dye molecules escape from the solid phase to the

solution with an increase the temperature. Similar findings were obtained for the adsorption of MG by Zeolite ZSM-5 [49], MO by modified montmorillonite nanomaterials [4], and MO by polyhydroxyl gemini surfactant-modified montmorillonite [32]. As a result, the ambient temperature was given the best-adsorbed amount, and it was selected as the optimum removal temperature for both dyes.

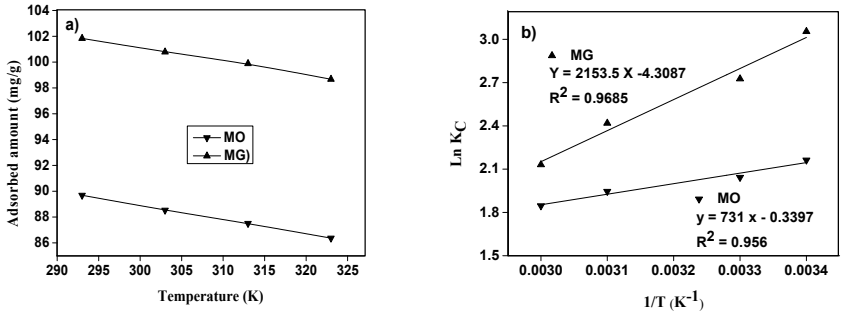

Figure 5. a) Effects of temperature on the MO and MG adsorption capacities of commercial bentonite (contact time: 20 min (MO) and 5 min (MG), pH = 2 (MO), adsorbent dose: 1 g/L (MO) and 0.6 g/L (MG)). b) Thermodynamic analysis for MO and MG adsorption by the commercial bentonite at different temperatures (adsorbate concentration = 100 mg/L, pH = 2 (MO), contact time: 20 min (MO) and 5 min (MG), adsorbent dose: 1 g/L (MO) and 0.6 g/L (MG)).

A thermodynamic parameter analysis was conducted to assess the Gibbs free energy (ΔG°), entropy (ΔS°), and enthalpy (ΔH°) based on the temperature investigation.

$$K_c = q_e m/C_e \quad (9)$$

$$\mathrm{Ln}K_c = \Delta S^{\circ}/R - \Delta H^{\circ}/RT \quad (10)$$

$$\Delta G^{\circ} = \Delta H^{\circ} - T\Delta S^{\circ} \quad (11)$$

where K_c is the thermodynamic equilibrium constant, q_e is the amount of dye adsorbed at equilibrium (mg/g), m is the adsorbent dose (g/L), Ce is the equilibrium concentration (mg/L) of the dye in solution, R is the universal gas constant (8.314 J/mol.K) and T is the absolute temperature (K). ΔH° and ΔS° are calculated from the slope ($-\Delta H^{\circ}/RT$) and intercept ($\Delta S^{\circ}/R$) of Van't Hoff scheme of $\mathrm{Ln}K_c$ versus 1/T (Figure 5b). Table 4 provides a summary of the thermodynamic parameters.

The values of ΔG° are negative at various temperatures, indicating that the adsorption of both dyes on commercial bentonite was a spontaneous process under the experimental conditions. The presence of a negative value for ΔH° indicates that the process of dye adsorption onto the adsorbent is exothermic. Additionally, the negative value of ΔS° denotes a decrease in the level of disorder at the interface between the solid and solution throughout the adsorption process. The determination of the magnitude of ΔH° can offer valuable insights into the underlying adsorption mechanism. Values below 40 kJ/mol are indicative of physical adsorption, while values beyond 40 kJ/mol suggest chemical adsorption [50]. The value of ΔH° in this study is below 40 kJ/mol, indicating that physical adsorption is the primary mechanism. The thermodynamic characteristics of the current material exhibit similarities to those reported in existing literature [4].

CONCLUSION

In this study, commercial bentonite from Biochem Chemopharma Company (France) was used to remove two dyes: methyl orange (anionic dye) and methyl green (cationic dye) from aqueous solutions. The material was characterized using XRF, FTIR, XRD, nitrogen adsorption at 77 K, and TGA. The factors such as contact time, solution pH, adsorbent amount, initial dye concentration, and temperature, influenced the adsorption process. Optimal parameters were determined: a contact time of 20 min for MO and 5 min for MG, pH of 2 for MO and natural pH for MG, adsorbent dose of 1g/L for MO, and 0.6 g/L for MG. The adsorption of MO followed pseudo-first-order kinetics. The Freundlich model fits best for MO, while both the Freundlich and Langmuir models fit well for MG. Thermodynamic studies showed that the adsorption is spontaneous, exothermic, and a physical process. Cationic dye exhibited better adsorption compared to anionic dye. Commercial bentonite can be considered a cost-effective and efficient adsorbent for cationic dyes in water treatment.

ACKNOWLEDGEMENTS

This work was supported by the Analysis Laboratory, Djilali Bounaama of Khemis-Miliana University (Algeria), and the Catalysis Laboratory, Castilla-La Mancha University (Spain).

REFERENCES

1. Guezzen, B.; Medjahed, B.; Benhelima, A.; Guendouzi, A.; Didi, M.A.; Zidelmal, S.; Boudia, R.A.; Adjdir, M. Improved pollutant management by kinetic and Box-Behnken design analysis of HDTMA-modified bentonite's adsorption of indigo carmine dye. *J. Ind. Eng. Chem*. **2023**, 125, 242-258.
2. Kayra Tanaydin, M.; Goksu, A. Optimization of the adsorption of methyl green dye on almond shells using central composite design. *Desalin. Water Treat*. **2021**, 227, 425-439.
3. Alardhi, S.M.; Albayati, T.M.; Alrubaye, J.M. Adsorption of the methyl green dye pollutant from aqueous solution using mesoporous materials MCM-41 in a fixed-bed column. *Heliyon* **2020**, 6, e03253.
4. Rezala, H.; Boukhatem, H.; Boudechiche, N.; Romero, A. Methyl orange adsorption by modified montmorillonite nanomaterials: Characterization, kinetic, isotherms and thermodynamic studies. *Indian J. Chem. Technol*. **2023**, 30, 85-93.
5. Ouachtak, H.; El Haouti, R.; El Guerdaoui, A.; Haounati, R.; Amaterz, E.; Addi, A.A.; Akbal, F.; Taha, M.L. Experimental and molecular dynamics simulation study on the adsorption of Rhodamine B dye on magnetic montmorillonite composite γ-Fe_2O_3@Mt. *J. Mol. Liq*. **2020**, 309, 113142.
6. Alalwan, H.A.; Sabti, N.; Ali, M.; Mohammed, M.M.; Mohammed, M.F.; Alminshid, A.H. A comparison study of methyl green removal by peroxi-coagulation and peroxi-electrocoagulation processes. *Clean. Eng. Technol*. **2023**, 13, 100623.
7. Rezala, H.; Douba, H.; Boukhatem, H.; Romero, A. Adsorption of methylene blue by hydroxyl-aluminum pillared montmorillonite. *J. Chem. Soc. Pak.* **2020**, 42, 550-563.
8. Alardhi, S.M.; Fiyadh, S.S.; Salman, A.D.; Adelikhah, M. Prediction of methyl orange dye (MO) adsorption using activated carbon with an artificial neural network optimization modeling. *Heliyon* **2023**, 9, e12888.
9. Lei, Y.; Liu, X.; Zhang, J.; Dai, Z.; Zhao, X.; Liu, G. A novel composite (ZIF-8@PEI-CC) with enhanced adsorption capacity and kinetics of methyl orange. *J. Solid State Chem.* **2023**, 318, 123758.

10. Farghali, A.A.; Bahgat, M.; El Rouby, W.M.A.; Khedr, M.H. Preparation, decoration and characterization of graphene sheets for methyl green adsorption. *J. Alloys Compd*. **2013**, 555, 193-200.
11. Naeem, A.; Saeed, Sayed, T.M.; Ahmad, B.; Mahmood, T.; Farooq, M.; Perveen, F. Chitosan decorated zirconium metal-organic framework for collaborative adsorption and photocatalytic degradation of methylene blue and methyl orange. *Process Saf. Environ. Prot.* **2023**, 176, 115-130.
12. Ewis, D.; Ba-Abbad, M.M.; Benamor, A.; El-Naas, M.H. Adsorption of organic water pollutants by clays and clay minerals composites: A comprehensive review. *Appl. Clay Sci.* **2022**, 229, 106686.
13. Rizzi, V.; Gubitosa, J.; Fini, P.; Romita, R.; Agostiano, A.; Nuzzo, S.; Cosma, P. Commercial bentonite clay as low-cost and recyclable "natural" adsorbent for the carbendazim removal/recover from water: Overview on the adsorption process and preliminary photodegradation considerations. *Colloids Surf. A: Physicochem. Eng. Asp.* **2020**, 602, 125060.
14. Magnoli, A.P.; Tallone, L.; Rosa, C.A.R.; Dalcero, A.M.; Chiacchiera, S. M.; Torres Sanchez, R.M. Commercial bentonites as detoxifier of broiler feed contaminated with aflatoxin. *Appl. Clay Sci*. **2008**, 40, 63-71.
15. Teixeira, S.C.G.; Oliveira, A.; Duarte, P.; Ferreira, L.F.V.; Moreira, J.C.; Peréz, D.V.; Marques, M.R.C. Pyrene photochemical species in commercial clays. *Chemosphere* **2013**, 90, 657-664.
16. AlTowyan, L.; AlSagabi, S., AlAjyan, T.; AlSulami, K.; Goumri-Said, S. The removal of manganese ions from industrial wastewater using local Saudi and commercial bentonite clays. *Groundw. Sustain. Dev.* **2022**, 19, 100821.
17. Boukhatem, H.; Ouazene, N.; Rezala, H.; Djouadi, L.; Selami1, S.; Zeraif, S. Removal of methylene blue dye from aqueous media by adsorption using nickel oxide modified montmorillonite composite. *Indian J. Chem. Technol.* **2023**, 30, 812-821.
18. Barrett, E.P.; Joyner, L.G.; Halenda, P.P. The determination of pore volume and area distributions in porous substances. I. computations from nitrogen isotherms. *J. Am. Chem. Soc.* **1951**, 73, 373-380.
19. Al-Zubaidi, N.S.; Alwasiti, A.A.; Mahmood, D. A comparison of nano bentonite and some nano chemical additives to improve drilling fluid using local clay and commercial bentonites. *Egypt. J. Pet.* **2017**, 26, 811-818.
20. Bukka, K.; Miller, J.D.; Shabtai, J. FTIR study of deuterated montmorillonite: structural features relevant to pillared clay stability. *Clays Clay Min.* **1992**, 40, 92-102.
21. Kumar, A.; Lingfa, P. Sodium bentonite and kaolin clays: Comparative study on their FT-IR, XRF, and XRD. *Mater. Today Proc.* **2020**, 22, 737-742.
22. Quero-Jiménez, P.C.; Arias Felipe, L.A.; Prieto García, J.O.; Jorge Rodríguez, M.E.; de la Torre, J.; Montenegro, O.N.; Molina-Ruiz, R.; Tiscornia, I.S. Local cuban bentonite clay: Composition, structure and textural characterization. *Andean Geol*. **2021**, 48, 546-556.
23. Dotto, G.L.; Vieillard, J.; Pinto, D.; Lütke, S.F.; Silva, L.F.O.; Dos Reis, G.S.; Lima, E.C.; Franco, D.S.P. Selective adsorption of gadolinium from real leachate using a natural bentonite clay. *J. Environ. Chem. Eng.* **2023**, 11, 109748.
24. Brunauer, S.; Deming, L.S.; Deming, W.E.; Teller, E. on a theory of the van der Waals adsorption of gases. *J. Am. Chem. Soc.* **1940**, 62, 1723-1732.
25. Sing, K.S.W.; Everett, D.H.; Haul, R.A.W.; Moscou, L.; Pierotti, R.A.; Rouquerol, J.; Siemieniewska, T. Reporting physisorption data for gas/solid systems with special reference to the determination of surface area and porosity. *Pure. Appl. Chem.* **1985**, 57, 603-619.
26. Kaufhold, S.; Dohrmann, R.; Klinkenberg, M.; Siegesmund, S.; Ufer, K. N_2-BET specific surface area of bentonites. *J. Colloid Interface Sci*. **2021**, 349, 275-282.

27. Alardhi, S.M.; Alrubaye, J.M.; Albayati, T.M. Adsorption of methyl green dye onto MCM-41: Equilibrium, kinetics and thermodynamic studies. *Desalin. Water Treat*. **2020**, 179, 323-331.
28. Lagergren, S. About the theory of so-called adsorption of soluble substances. *K. Sven. Vetenskapsakademiens Handl.* **1898**, 24, 1-39.
29. Ho, Y.S.; McKay, G. Kinetic models for the sorption of dye from aqueous solution by wood. *Process Saf. Environ. Prot.* **1998**, 76, 183-191.
30. Ho, Y.S.; McKay, G. Pseudo-second order model for sorption process. *Process Biochem.* **1999**, 34, 451-465.
31. Gil, A.; Assis, F.C.C.; Albeniz, S.; Korili, S.A. Removal of dyes from wastewaters by adsorption on pillared clays. *Chem. Eng. J.* **2011**, 168, 1032-1040.
32. Peng, S.; Zheng, C.; Wu, X.; Wei; Y.; Zeng, Z.; Xiao, R.; Sun, Y. Polyhydroxyl gemini surfactant-modified montmorillonite for efficient removal of methyl orange. *Colloids Surf. A: Physicochem. Eng. Asp.* **2019**, 578, 123602.
33. Chen, D.; Chen, J.; Luan, X.; Ji, H.; Xia Z. Characterization of anion–cationic surfactants modified montmorillonite and its application for the removal of methyl orange. *Chem. Eng. J.* **2011**, 171, 1150-1158.
34. Rytwo, G.; Nir, S.; Crespin, M.; Margulies, L. Adsorption and interactions of methyl green with montmorillonite and sepiolite. *J. Colloid Interface Sci.* **2000**, 222, 12-19.
35. Dos Reis, L.G.T.; Robaina, N.F.; Pacheco, W.F.; Cassella, R.J. Separation of malachite green and methyl green cationic dyes from aqueous medium by adsorption on amberlite XAD-2 and XAD-4 resins using sodium dodecylsulfate as carrier. *J. Chem. Eng.* **2011**, 171, 532-540.
36. Qiao, J.; Gao, S.; Yao, J.; Zhang, L.; Li, N.A. Rapid and green method for the removal of anionic dyes from aqueous solution using sulfobetaine-modified magnetic nanoparticles. *AIP Adv.* **2019**, 9, 065308.
37. Jalal, A.F.; Fakhre, N.A. Removal of dyes (BG, MG, and SA) from aqueous solution using a novel adsorbent macrocyclic compound. *PLoS One* **2022**, 17, e0275330.
38. Adebayo, M.A.; Adebomi, J.I.; Abe, T.O.; Areo, F. Removal of aqueous Congo red and malachite green using ackee apple seed–bentonite composite. *Colloids Interface Sci. Commun.* **2020**, 38, 100311.
39. Langmuir, I. The constitution and fundamental properties of solids and liquids. *J. Am. Chem. Soc.* **1916**, 38, 2221-2295.
40. Freundlich, H.M.F. Uber die adsorption in Losungen. *Z. Phys. Chem.* **1906**, 57, 385–470.
41. Temkin, M.J.; Pyzhev, V. Recent modifications to Langmuir isotherms. *Acta Physiochim. URS* **1940**, 12, 217-225.
42. Singh, K.; Kumar, A.; Singh, A.K.; Agarwal, A. Fly ash and TiO_2 modified fly ash as adsorbing materials for effective removal of methylene blue and malachite green from aqueous solutions. *J. Indian Chem. Soc.* **2023**, 100, 100942.
43. Bahgat, M.; Farghali, A.A.; El Rouby, W.; Khedr, M.; Mohassab, Y.; Mohassab, A. Adsorption of methyl green dye onto multi-walled carbon nanotubes decorated with Ni nanoferrite. *Appl. Nanosci.* **2013**, 3, 251-261.
44. Tang, X.; Li, Y.; Chen, R.; Min, F.; Yang, J.; Dong, Y. Evaluation and modeling of methyl green adsorption from aqueous solutions using loofah fibers. *Korean J. Chem. Eng.* **2014**, 32, 125-131.
45. Atshan, A.A. Adsorption of methyl green dye onto bamboo in batch and continuous system. *IGCPE* **2014**, 15, 65-72.
46. Ansari, M.J.; Jasim, S.A.; Bokov, D.O.; Thangavelu, L.; Yasin, G.; Khalaji, A.D. Preparation of new bio-based chitosan/Fe_2O_3/$NiFe_2O_4$ as an efficient removal of methyl green from aqueous solution. *Int. J. Biol. Macromol.* **2022**, 198, 128-134.

47. Nayak, S.; Goveas, L.C.; Selvaraj, R.; Mutalik, S.; Sajankila, S.P. Use of *Cyclea peltata* mediated gold nanospheres for adsorptive degradation of methyl green dye. *Bioresour. Technol.* **2022**, 20, 101261.
48. Shouman, M.; Khedr, S. Removal of cationic dye from aqueous solutions by modified acid-treated pomegranate peels (*Punica granatum*): Equilibrium and kinetic studies. *Asian J. App. Sci.* **2015**, 3, 1-15.
49. Maaza, L.; Djafri, F.; Bouchekara, M.; Djafri, A. Adsorption of methyl green onto zeolite ZSM-5 (pyrr.) in aqueous solution. *Orient. J. Chem*. **2016**, 32, 171-180.
50. Wang, K.; Kou, Y.; Wang, K.; Liang, S.; Guo, C.; Wang, W.; Lu, Y.; Wang, J. Comparing the adsorption of methyl orange and malachite green on similar yet distinct polyamide microplastics: Uncovering hydrogen bond interactions. *Chemosphere* **2023**, 340, 139806.